Available online at www.sciencedirect.com

ScienceDirect

Ceramics International 40 (2014) 541–549

CERAMICS INTERNATIONAL

www.elsevier.com/locate/ceramint

Influence of SiC additive on the ablation behavior of C/C composites modified by ZrB_2–ZrC particles under oxyacetylene torch

Lei Liu, Hejun Li*, Xiaohong Shi, Qiangang Fu, Wei Feng, Xiyuan Yao, Chang Ni

State Key Laboratory of Solidification Processing, Northwestern Polytechnical University, Xi'an 710072, Shaanxi, PR China

Received 29 April 2013; received in revised form 11 June 2013; accepted 11 June 2013
Available online 18 June 2013

Abstract

To determine the effect of SiC additive on the ablation behavior of carbon/carbon composites modified by ZrB_2–ZrC particles (C/C–Z), C/C–Z and C/C–Z with SiC additive (C/C–Z–SiC) were ablated by oxyacetylene torch for different times up to 240 s. Results showed the improved ablation property of C/C–Z–SiC in comparison with C/C–Z during the initial 120 s but depletion of the improvement with the ablation further proceeding. Meanwhile, the recorded surface temperature of C/C–Z–SiC was lower than that of C/C–Z under the same ablation condition during the initial 160 s after which they tended to be the same. The ablated surface center morphology of C/C–Z–SiC implied that a SiO_2 rich layer was formed beneath the chalked ZrO_2 outer layer within 120 s ablation while the SiO_2 rich layer was almost depleted beyond 240 s. The formation and depletion of SiO_2 rich layer from oxidation of SiC additive dominated the distinct ablation behaviors of C/C–Z–SiC and C/C–Z.

Keywords: D. SiC; Carbon/carbon composites; Ablation; ZrB_2

1. Introduction

Ultra high temperature ceramics (UHTCs) modified carbon/carbon (C/C) composites for improving the ablation resistance have been largely reported in the last two decades. Among these works, ZrB_2–ZrC (Z) modified C/C composites (C/C–Z) have attracted increasing attention and many methods have been attempted to fabricate the composites. All methods, including slurry infiltration [1,2], precursor infiltration and pyrolysis (PIP) [3,4], reactive melt infiltration (RMI) [5–7], chemical vapor decomposition [8], thermal spray technology [9] and combination of them [10,11], have been successfully used to prepare C/C–Z composites. Meanwhile, the ablation properties of pitch-derived ZrC/C composites [12], C/C–ZrC composites [13] and C/C–ZrB_2 [14] composites were evaluated by oxyacetylene torch, showing a better ablation resistance than that of pristine C/C composites as more ingredients of UHTCs were added. C/C–ZrC [5,6] ablated by laser also displayed a better ablation property than C/C and C/SiC composites. Besides, C/ZrC composites showed a four-layer microstructure after ablation by oxyacetylene torch [15]. Recently, many investigations have concentrated on the ablation behavior of C/C–Z with SiC additive (C/C–Z–SiC) [16–18]. Some studies suggested that SiC additive could improve the ablation property of Z or Z modified C/C composites [19,20] since the melted SiO_2 could fill in the porous ZrO_2 and block the infiltration of oxidizing species. Nevertheless, some other researches showed that the SiC additive led to more serious ablation of C/C–Z [1,2]. Because there have been few works making a direct comparison between C/C–Z–SiC and C/C–Z composites, it is hard to assess whether the SiC additive is beneficial to the improvement of ablation property of C/C–Z or not. In other words, the effect of SiC on the ablation of C/C–Z is still unclear. Therefore, we believe it is necessary and meaningful to clarify the ablation mechanism in order to optimize the composition of UHTCs modified C/C composites.

*Corresponding author. Tel.: +86 29 88495004; fax: +86 29 88492642.
E-mail address: lihejun@nwpu.edu.cn (H. Li).

0272-8842/$ - see front matter © 2013 Elsevier Ltd and Techna Group S.r.l. All rights reserved.
http://dx.doi.org/10.1016/j.ceramint.2013.06.036

In the present work, Z and Z–SiC particles were deposited into carbon fiber fabric using the traditional PIP process and then the doped fabrics were densified by pyrocarbon and finally graphitized. To understand how SiC works during the ablation of Z modified C/C composites, C/C, C/C–Z and C/C–Z–SiC (with the same Z concentration as C/C–Z) were ablated by oxyacetylene torch with a relative low heat flux of $2.38 \pm 10\%$ MW/m^2 for different times until termination at 240 s. The comparison of ablation rates, recorded surface temperatures and ablated morphologies of the prepared composites provided a good guidance to understand the ablation mechanism of C/C–Z–SiC.

2. Experimental procedure

2.1. Composite preparation

Ceramic particles were deposited into T300 PAN-based carbon fiber fabricated needle punched disk felts (0.45 g/cm^3) by the traditional PIP process using a certain amount of organic Z precursor (purchased from Chinese Academy of Sciences, ceramic production ratio was about 33 wt%) and polycarbosilane (PCS, ceramic production ration was about 64 wt%) in dimethylbenzene solution. After immersion under vacuum for 20 min, impregnated felts were taken out and dried in a drying oven at 90 °C for 24 h. Afterward, the dried carbon felts were heat treated in a flowing Ar atmosphere at 1400–1800 °C for 2 h. In the heat treatment process, Z and SiC particles were formed in the carbon fiber felts. The mass of ceramic particles in each felt was calculated according to

$$m_{ceramic} = m_1 - m_0 \quad (1)$$

where m_0 and m_1 are the masses of carbon felt before impregnation and after heat treatment, respectively. For comparison, the felts of C/C–Z and C/C were heat treated together with those of C/C–Z–SiC.

When the expected ceramic content was achieved, all the carbon felts were densified through a thermal gradient chemical vapor infiltration (TCVI) process at 950–1150 °C for 110 h using methane as a carbon source. After the final step of graphitizing at 2200–2500 °C for 2 h in a flowing Ar atmosphere, ceramic-modified C/C composites and pure C/C composites were fabricated. The total mass percentage of Z–SiC particles in C/C–Z–SiC (1.87 g/cm^3) was about 10.0% (ratio of $m_{ceramic}$ and the final mass of relative composites) while the mass ratio (Z:SiC) was 3:2. Moreover, the mass percentage of Z in C/C–Z (1.89 g/cm^3) was about 6.1% which is the same as that of Z in C/C–Z–SiC.

Disk samples (∅30 mm × 10 mm) were cut from the prepared composites and lightly abraded with 80 and 400 grit SiC paper before ablation test.

2.2. Ablation test and characterization

The ablation test was carried out under oxyacetylene torch with a heat flux of $2.38 \pm 10\%$ MW/m^2 according to Tang et al. [1] for different times. The inner diameter of the oxyacetylene gun tip was 2 mm and the distance from the gun tip to the sample was 10 mm. The ablation angle was 90°. Other parameters about the O_2 and C_2H_2 were displayed in Table 1.

Table 1
Parameters of O_2 and C_2H_2 for the ablation test.

	Pressure (MPa)	Flux (L/s)
O_2	0.4	0.24
C_2H_2	0.095	0.18

The linear and mass ablation rates were calculated according to Eqs. (2) and (3). The ultimate data was the average of three samples.

$$R_l = \frac{\Delta d}{t} \quad (2)$$

$$R_m = \frac{\Delta m}{t} \quad (3)$$

R_l is the linear ablation rate; Δd is the change of the sample's thickness at central region before and after ablation; R_m is the mass ablation rate; Δm is the sample's mass change before and after ablation; and t is the ablation time.

The surface temperature was measured by an infrared thermometer (Raytek MR1SCSF) in 2-color mode with an error of $\pm 0.75\%$.

The phase analysis of prepared composites before and after ablation was conducted by X-ray diffraction (XRD, X'Pert Pro MPD). Morphologies and chemical compositions of the prepared and ablated composites were investigated by scanning electron microscopy (SEM, JSM6460) combined with energy dispersive spectroscopy (EDS).

3. Results and discussion

3.1. Microstructure and ablation property

Fig. 1 shows the cross-section morphology of the prepared samples and the corresponding EDS analysis. It is shown that the doped ceramic particles are embedded in the carbon matrix in the high magnified SEM (left inferior corner of Fig. 1(b)) where the white phase is Z, the gray phase is SiC and the black phase is carbon (C). These results were also confirmed by EDS analysis. In the lower magnification SEM images, we can find that the fine ceramic particles are distributed uniformly in the cross-section of both composites. The uniform micro-structure would contribute to the persistent anti-ablation property which is helpful to predict the lifespan of component in practical application. The EDS mapping analysis elucidates the element constitution of the two composites: C/C–Z consists of C and Zr while C/C–Z–SiC is comprised of C, Si and Zr. No other impurities were detected. The absence of B in the mapping analysis is attributed to the inherent characteristic of light element.

Fig. 2 shows the ablation rates of different composites versus ablation time. It is easy to find that the modified C/C

composites have lower ablation rates than pure C/C composites. In other words, the ablation properties of C/C composites under oxyacetylene torch with the heat flux of 2.38 MW/m^2 have been improved by doped particles. However, C/C composites display a relatively stable ablation property in terms of both linear and mass ablation rates at prolonged ablation time. In contrast, the linear ablation rates of modified C/C composites decline sharply from 60 to 120 s. Afterward, the decreasing trend of linear ablation rates for C/C–Z slows as the ablation proceeds. Meanwhile, for C/C–Z–SiC, there is an abnormal rise of linear ablation rate from 120 to 180 s beyond which a slight decline occurs. As a result, linear ablation rates of C/C–Z and C/C–Z–SiC tend to be similar in the 240 s ablation. On the other hand, the mass ablation rates of C/C–Z–SiC are lower than those of C/C–Z during the initial 120 s ablation. When ablation time is longer than 180 s, the mass ablation rates of the two modified C/C composites are approaching the same. Combined with the uniform microstructure of the two modified C/C composites, it can be inferred that the accumulation of ablation products generated from Z and Z–SiC particles on the ablated surface is intimately associated with their ablation properties versus ablation time.

3.2. Temperature

Fig. 3 shows the photo of oxyacetylene torch test rig and the plot of surface temperature versus ablation time measured by an infrared thermometer (Raytek MR1SCSF) in 2-color mode. During ablation, the sample was fixed in a water cooled copper holder. Accordingly, the temperature gradient from sample center to its border region can be inferred depending on the basic thermal conduction theory. The most seriously destroyed region at the center in many related researches [21–23] also proves the recorded surface temperature in Fig. 3(b) to be the temperature of surface center of the ablated sample.

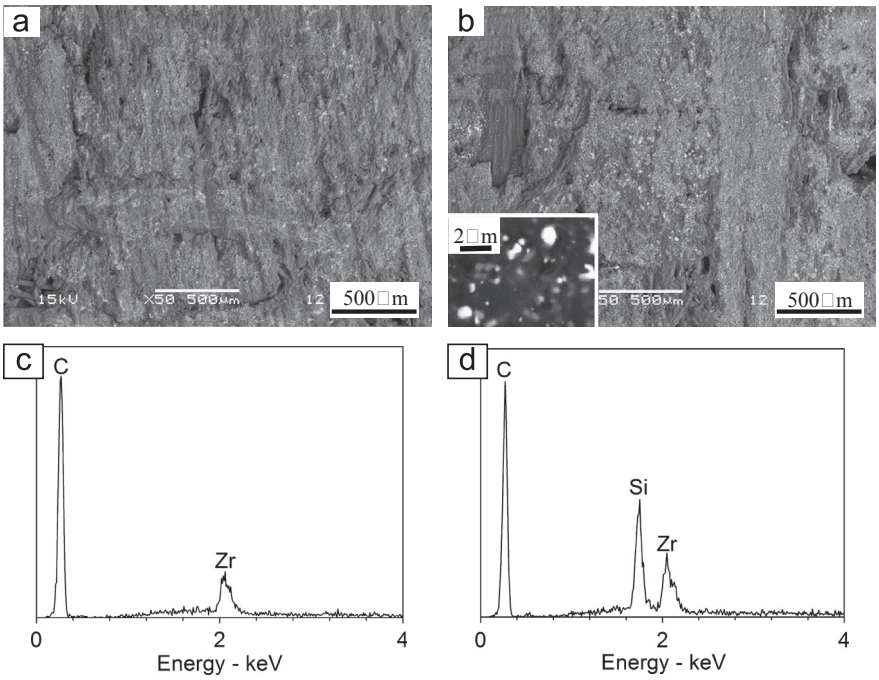

Fig. 1. Cross-section morphology of prepared samples and corresponding EDS analysis: (a) C/C–Z; (b) C/C–Z–SiC; (c) mapping to (a); and (d) mapping to (b).

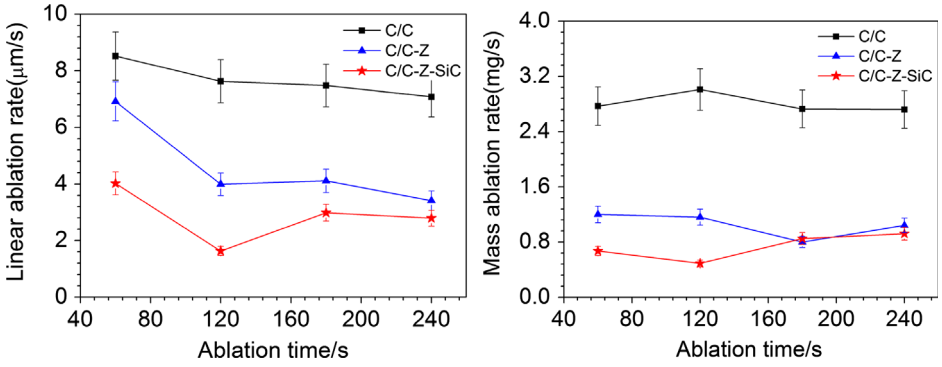

Fig. 2. Ablation rates of different composites versus ablation time.

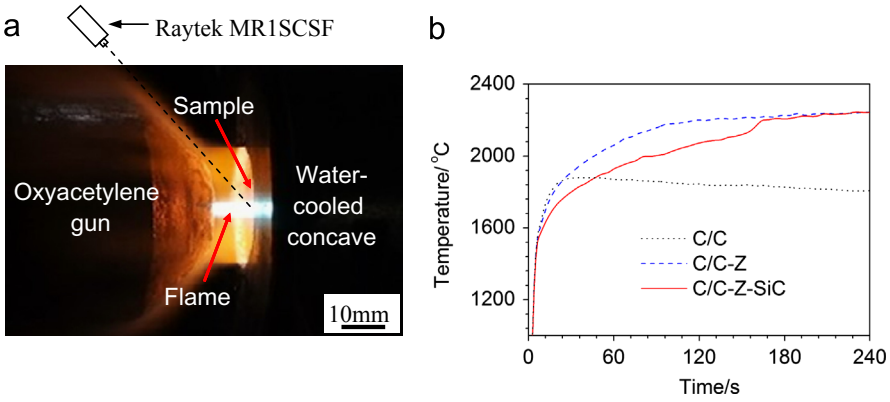

Fig. 3. Photo of oxyacetylene torch test rig (a) and the plot of surface temperatures versus ablation time during test (b).

In Fig. 3(b), we can find that the surface temperature of C/C composites increases fast to the top point and then remains at a relatively stable level with a much lower value than that of C/C–Z or C/C–Z–SiC. The surface temperature of C/C–Z also rises up to a stable value after being ablated for 120 s. For C/C–Z–SiC, the surface temperature increases continuously until 160 s and reaches the same plateau as that of C/C–Z. Comparing the above results from these three kinds of composites tested in the same heating condition by oxyacetylene torch, it is deduced that the higher surface temperature of modified C/C composites is caused by the doped ceramic particles. The SiC additive accounts for the different surface temperatures of C/C–Z and C/C–Z–SiC. Moreover, the recorded surface temperatures between 0 and 120 s in the present work are coincident with those of C/C sample, C_f–ZrB_2 and C_f–ZS20 reported by Paul et al. [2].

To further understand the recorded surface temperature of the ablated samples, the macro-morphology of the oxyacetylene torch is shown in Fig. 4. The oxyacetylene torch consists of three parts: inner cone, outer envelope and acetylene feather, which is the same as the profile of oxyacetylene torch [24]. The oxyacetylene torch can be adjusted by the ratio of oxygen/acetylene to different functionalities: carbonizing, neutral or oxidizing. Ours is oxidizing flame with the ratio of oxygen/acetylene specified in Table 1, having the highest temperature among the three flames. The inner cone where acetylene and oxygen are mixed is the hottest part of the torch. And it is well known that temperature of the inner cone is as high as 3000 °C [8,19,24] while temperature of the outer envelope is just about 150 °C [24]. Considering the 5 mm diameter of inner cone compared with the 30 mm diameter of ablated sample, the temperature gradient of oxyacetylene torch should be another reason for the most seriously ablated sample center except for the water cooled wall of sample holder.

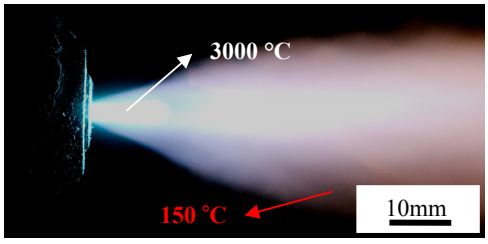

Fig. 4. Macro-morphology of the oxyacetylene torch.

3.3. Ablated samples

Fig. 5 shows the cross-sectional macro-morphology of the ablated C/C–Z and C/C–Z–SiC samples. In both cases of 120 and 240 s ablation, the white layer of ablation products on the front face of C/C–Z is incomplete since a concave dent (marked as region A) formed in the center. Contrarily, the surface of C/C–Z–SiC is covered by a well-defined white layer after being ablated for 120 s, although some holes which provide the channel for $CO/CO_2/B_2O_3/SiO_2$ to overflow exist. However, when ablated over 240 s, the integrated layer of ablation products was eventually broken down due to the further erosion. Consistent with the results of the ablation rates in Fig. 2, it can be inferred that the SiC additive loses its effect in improving the ablation property of C/C–Z in continuous ablation up to 240 s.

Since the recorded surface temperature of C/C–Z and C/C–Z–SiC rose to above 2000 but below 2300 °C, all the following reactions possibly occurred on the surface of ablated samples during ablation depending on the basic thermal chemical principles:

$$2C\ (s) + O_2(g) \rightarrow 2CO\ (g) \quad (4)$$

$$2SiC\ (s) + 3O_2(g) \rightarrow 2SiO_2(l) + 2CO\ (g) \quad (5)$$

$$2ZrB_2(s) + 5O_2(g) \rightarrow 2ZrO_2(s) + 2B_2O_3(l) \quad (6)$$

$$2ZrC\ (s) + 3O_2(g) \rightarrow 2ZrO_2(s) + 2CO\ (g) \quad (7)$$

$$SiO_2(l) \rightarrow SiO_2(g) \quad (8)$$

$$B_2O_3(l) \rightarrow B_2O_3(g) \quad (9)$$

Under the constant high temperature and oxidative condition, the accumulated SiO_2 in the prophase of ablation would evaporate and be depleted gradually. This should be the main reason for the damage of ablation products layer of C/C–Z–SiC after 240 s ablation.

Fig. 6 shows the XRD patterns of C/C–Z and C/C–Z–SiC before and after ablation. Before ablation, C/C–Z is composed of ZrB_2, ZrC and C while C/C–Z–SiC is comprised of ZrB_2, ZrC, C and SiC. Moreover, the relative intensity ratio of ZrB_2 to ZrC peaks (RPZ) is different in these two composites, which is caused by the influence of PCS on the pyrolysis of organic Z precursor. After ablation, ZrO_2 appears in both composites. The RPZ of C/C–Z–SiC remains the same as that before ablation whereas that of C/C–Z decreases, indicating faster consumption of ZrB_2 in C/C–Z than that in C/C–Z–SiC under the same oxyacetylene torch with the heat flux of 2.38 MW/m^2. In other words, the SiC additive could slow down the consumption of ZrB_2 compared with ZrC in the present test. Moreover, no SiO_2 is detected in the XRD analysis because fast cooling after ablation induces the poor crystalline state of residual SiO_2. It is also found that although the macro-morphologies of C/C–Z–SiC are different for 120 and 240 s cases, there is almost no difference between their phases.

3.4. How SiC works during ablation

Fig. 7 shows the surface central morphology of C/C–Z samples after ablation (high magnification of region A in Fig. 5) and corresponding EDS analysis. The ablated surface center of C/C–Z is similar in both cases of 120 and 240 s ablation. In the original morphology after ablation (Fig. 7(a)), we can find that some white particles are embedded in black phase. EDS analysis of Spot 1 indicates that the white particles are ZrO_2. And the black phase was proved to be carbon. After being lightly cleaned by gas flow, it was observed that the

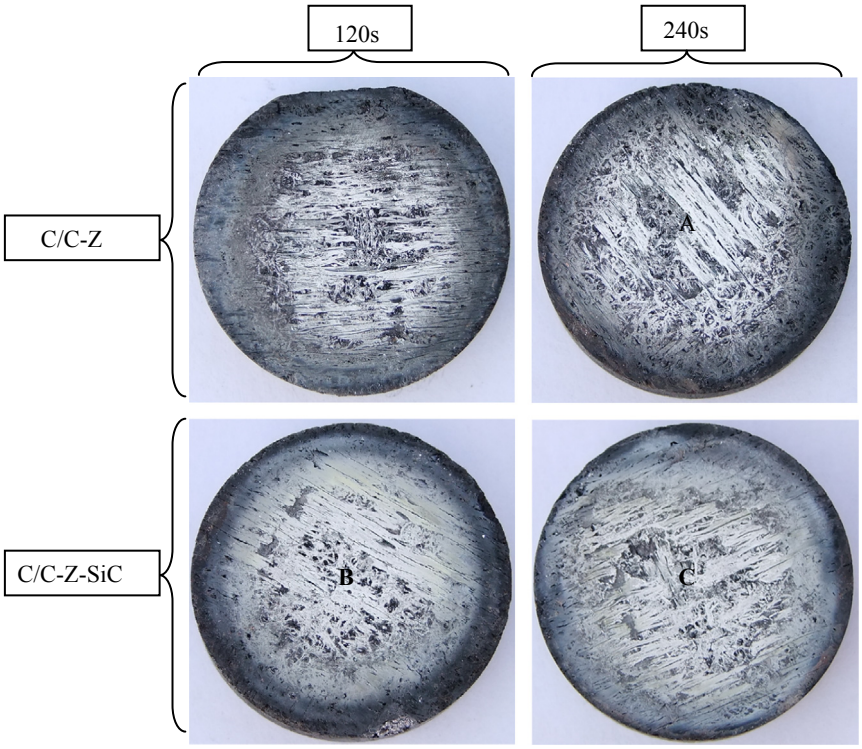

Fig. 5. Cross-sectional macro-morphology of samples after ablation for different times.

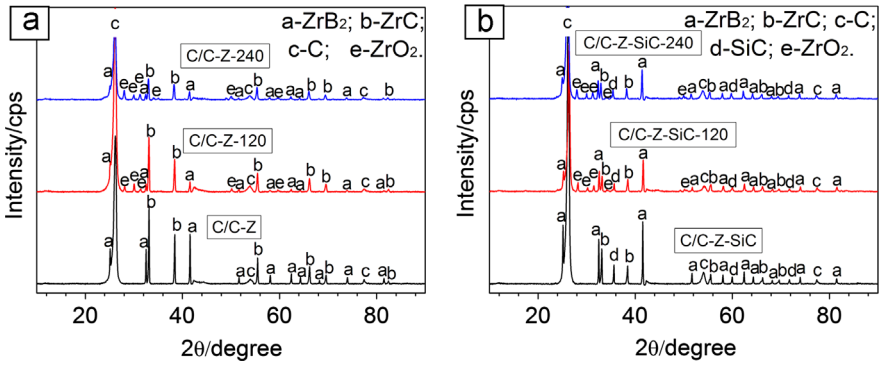

Fig. 6. XRD patterns of C/C–Z and C/C–Z–SiC before and after ablation.

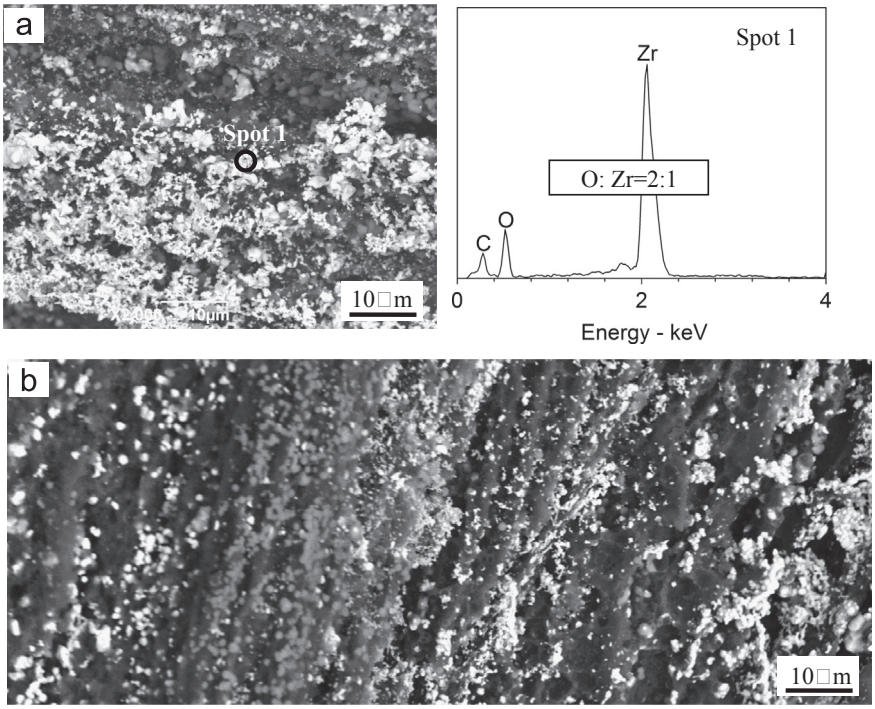

Fig. 7. Surface central morphology of C/C–Z samples after ablation (high magnification of region A in Fig. 5) and corresponding EDS analysis: (a) original morphology; and (b) after being lightly cleaned by gas flow.

amounts of white particles become fewer on the surface center of C/C–Z (Fig. 7(b)). Differently, the residual white particles are not pure ZrO_2 but a mixture with co-existing ZrB_2 and ZrC (confirmed by EDS analysis). Moreover, in the wide field of vision (Fig. 7(b)), the surface is not smooth. Some protruding parts and a lot of pits and holes can be found. Thus, it is a porous layer that is composed of ZrO_2 and Z and covered on the front face of C/C–Z. Although the anti-ablation property of C/C–Z is better than that of C/C composites, it seems that the layer of ablation products cannot block the infiltration of oxidizing species effectively due to its porous micro-structure.

Fig. 8 shows the surface central morphology of C/C–Z–SiC samples after being ablated for 120 s (high magnification of region B in Fig. 5) and corresponding EDS analysis. It is obvious that the accumulated Z particles on the surface of C/C–Z–SiC (Fig. 8(a)) were not oxidized completely (EDS analysis of Spot 1 in Fig. 8) and some of these particles were sintered during ablation (Fig. 8(a)). Moreover, there are two different morphologies in Fig. 8(a) marked as regions D and E. As mentioned in Section 3.3, some holes exist in the white layer of ablated C/C–Z–SiC surface. The region E is the transition part connecting the white layer to the holes. EDS analysis of Spots 1 and 2 indicate that a little SiC or SiO_2 is left in the region E whereas no Si is detected in the region D. Compared with ablation morphology of C/C–Z (Fig. 7(a)), the morphology in region D suggests that the existence of SiC/SiO_2 accelerates the sintering of Z/ZrO_2 during ablation. When the white layer is lightly peeled off by gas flow, the sub-layer displays a similar morphology to the bottom of the hole in the exterior white layer. EDS of Spot 3 confirms that the sub-layer consists of SiO_2 with few ZrO_2 relying on the stoichiometry of O/(Zr+Si) and the O element in the sub-layer is excessive. Besides, the SiO_2 rich layer should melt or partially melt during ablation depending on its morphology (Fig. 8(b)).

After being ablated for 240 s, the surface central morphology of C/C–Z–SiC samples (region C in Fig. 5) and corresponding EDS analysis are shown in Fig. 9. The ablated samples are covered by partial sintered ZrO_2/Z particles with a little SiC/SiO_2 (Fig. 9(a)). This is the same as that in region D of Fig. 8(a). However, the particles become larger and some micro-holes come into being in the exterior layer. After the particles are lightly cleaned by gas flow, a concave sub-layer can be found (Fig. 9(b)). EDS analysis of Spots 2 and 3 indicates that only SiC, Z and C are left while no ZrO_2 or SiO_2 is detected in the sub-layer. In other words, the SiO_2 rich layer is completely depleted.

3.5. Ablation mechanism of modified C/C composites

It has been studied that the oxidizing chemical composition of oxyacetylene torch is O_2, CO_2, CO, O, OH and H_2O [13]. During ablation, the surface center of the ablated sample is heated by the stable oxidizing gas flow at 3000 °C. With prolonging of test time, the ablation of modified C/C composites tends to balance no matter what in the view of heat transfer (surface temperature) or mass transfer (accumulation and consumption of ablation products on the ablated surface). Thus the ablation of C/C–Z or C/C–Z–SiC can be divided into several steps.

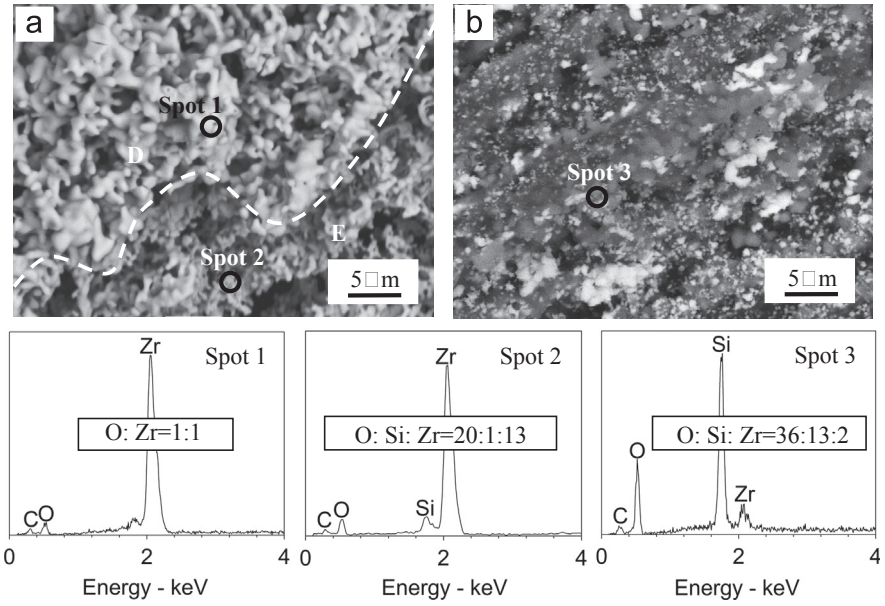

Fig. 8. Surface central morphology of C/C–Z–SiC samples after ablation for 120 s (high magnification of region B in Fig. 5) and corresponding EDS analysis: (a) original morphology; and (b) after being lightly cleaned by gas flow.

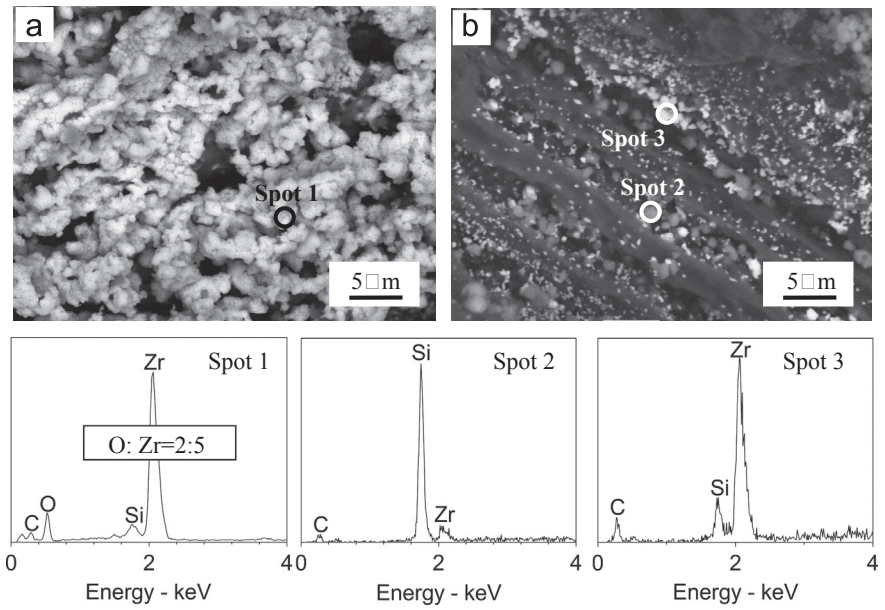

Fig. 9. Surface central morphology of C/C–Z–SiC samples after ablation for 240 s (high magnification of region C in Fig. 5) and corresponding EDS analysis: (a) original morphology; and (b) after being lightly cleaned by gas flow.

For C/C–Z, the ablation can be divided into two steps. Firstly, the composites are oxidized and the oxidation proceeds faster at the interface of fiber/matrix or C/Z than other parts. Then mechanical erosion will occur when the strength of micro-components at the surface of ablated sample decreases to a certain degree. Meanwhile, ZrO_2 from the oxidizing of Z accumulates on the surface. The accumulation induces the formation of the protective white layer, which could decline the ablation rates and raise the surface temperature. This process continues for about 120 s according to the change of ablation rates (Fig. 2) or surface temperature (Fig. 3). Secondly, the accumulation and consumption (mechanical erosion) of ZrO_2+Z on the surface comes into a balance, which dominates the slight decrease of ablation rates. Meanwhile, as the surface chemical composition of C/C–Z becomes invariable, the heat from oxyacetylene torch tends to be equal to the thermal radiation plus the thermal conduction of sample. Thus, the surface temperature becomes steady after being ablated for 120 s.

The ablation of C/C–Z–SiC can be divided into three steps. Firstly, ZrO_2 and SiO_2 from oxidation of Z and SiC accumulate on the surface of C/C–Z–SiC. After being ablated for 60 s,

the partially covered surface by ball like ZrO_2+SiO_2 demonstrated that the accumulation is not completed [25]. Since the temperature of inner cone of oxyacetylene torch is as high as 3000 °C, the SiC/SiO_2 in the outer surface will decompose [26,27] or volatilize. This should be the main reason for the formation of ZrO_2+Z outer layer without SiC/SiO_2 after being ablated for 120 s (Fig. 8(a)). Because ZrO_2 has a low thermal conductivity, temperature of the sub-layer is lower than the detected temperature. This makes it possible for the formation of SiO_2 rich sub-layer (Fig. 8(b)). In this process, the increase of SiO_2 in the sub-layer could fill in the defects of substrate and cover on that. And then the SiO_2 rich layer could protect C/C–Z–SiC from fast oxidizing, which prompts the decrease of ablation rates in the initial 120 s ablation. Secondly, the surface temperature rises further and the temperature of the sub-layer also increases. The increase of sub-layer's temperature accelerates the volatilization of SiO_2 due to the relationship between vapor pressure of SiO_2 and temperature [28,29]. As a result, the linear ablation rates of C/C–Z–SiC show an abnormal raise from 120 to 180 s and the relative mass ablation rates also increase. Finally, the SiO_2 rich sub-layer is depleted and the front face of C/C–Z–SiC is covered by ZrO_2+Z. The similar surface chemical composition of C/C–Z–SiC and C/C–Z leads to their close surface temperature. It is obvious that the SiC additive prompts the formation of SiO_2 rich sub-layer and decreases the ablation rates in the incipient ablation whereas it loses its protective effect gradually in the durative high temperature ablation. In a word, the SiC additive in C/C–Z prolongs the process that mass and heat transfer went to a balance.

Fig. 10 shows the schematic diagram of ablation of prepared composites in heat flux of 2.38 MW/m^2 under oxyacetylene torch. We can find the structure of ablated C/C–Z (Fig. 10(a)). In comparison with the structure of ablated C/ZrC composite [15], the melting layer of ZrO_2 was not found in the ablated C/C–Z. By investigating the peeled particles collected below the ablated samples during test, some melting ZrO_2 was detected. Thus, the absence of melting ZrO_2 layer should come from the following three reasons. First, the matrix of the C/C–Z consists of pyrocarbon and low content of Z while the matrix of C/ZrC is complete ZrC. The amount of Z in C/C–Z is not enough to form an integrated ZrO_2 layer while it is continuously peeled off by gas flow, the same as the sample of Zr-1.40 in research [17]. Second, the surface temperature is lower than the melting point of ZrO_2. Thus a visible melting ZrO_2 layer may not be formed. Third, some particles fell off from the ablated surface of C/C–Z during cooling as a result of the phase transition of ZrO_2. The melting ZrO_2 may disappear from the surface in this process. Similarly, the melting layer was not detected on the ablated surface of C/C–Z–SiC. Besides, the SiC depleted layer in ablated 3D C/ZrC–SiC [19] was not found in the ablated C/C–Z–SiC, either. This is consistent with the surface central microstructure of ablated C/C–ZrC–SiC composites [17,30]. The low content of SiC in the matrix and the large amount of pyrocarbon under the ablated surface possibly account for that.

4. Conclusion

C/C, C/C–Z and C/C–Z–SiC were ablated by oxyacetylene torch with a heat flux of 2.38 MW/m^2 for different times up to 240 s in the present work. The C/C–Z–SiC possessed an improved ablation property compared with C/C–Z during the initial 120 s and the improvement was depleted with further developing of ablation. Meanwhile, the recorded surface temperature of C/C–Z–SiC was lower than that of C/C–Z in the incipient 160 s ablation and then their surface temperatures tended to be the same. The morphology of the ablated surface center suggested that a SiO_2 rich layer was formed beneath the chalked ZrO_2 outer layer in C/C–Z–SiC within 120 s ablation while the SiO_2 rich layer was almost depleted beyond 240 s.

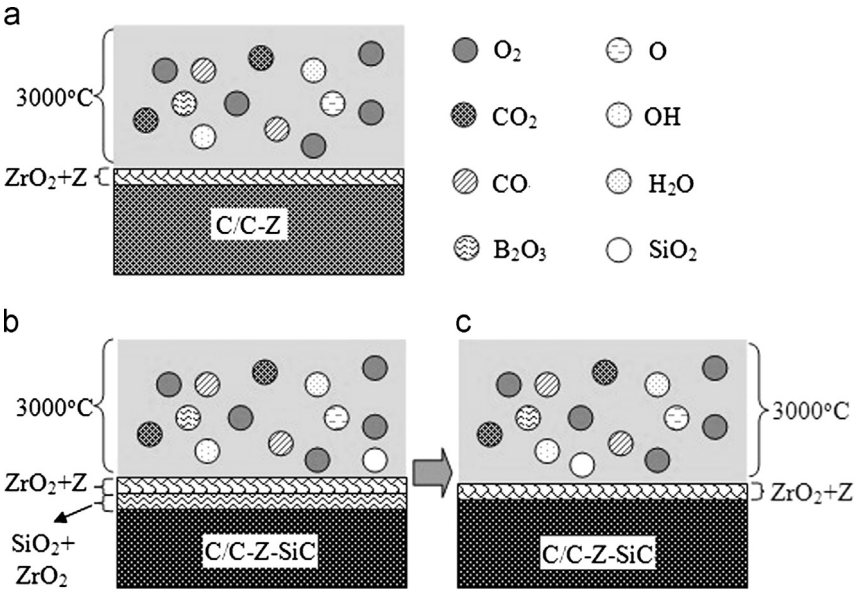

Fig. 10. Schematic diagram of ablation of prepared composites in a heat flux of 2.38 MW/m^2 under oxyacetylene torch: (a) C/C–Z; (b) C/C–Z–SiC for a short term ablation; and (c) C/C–Z–SiC for a long term ablation.

The formation and depletion of SiO_2 rich layer from oxidation of SiC additive dominated the distinct ablation behaviors of C/C–Z–SiC and C/C–Z.

Acknowledgments

This work has been supported by the National Natural Science Foundation of China under Grant nos. 51202093 and 51221001, the Fundamental Research Foundation of Northwestern Polytechnical University under Grant no. GBKY1021, the Research Fund of State Key Laboratory of Solidification Processing (NWPU), China (Grant no. 25-TZ-2009) and the "111" Project under Grant no. B08040.

References

[1] S.F. Tang, J.Y. Deng, S.J. Wang, W.C. Liu, K. Yang, Ablation behaviors of ultra-high temperature ceramic composites, Materials Science and Engineering: A 465 (2007) 1–7.
[2] A. Paul, S. Venugopal, J.G.P. Binner, B. Vaidhyanathan, A.C.J. Heaton, P.M. Brown, UHTC-carbon fibre composites: preparation, oxyacetylene torch testing and characterization, Journal of the European Ceramic Society 33 (2013) 423–432.
[3] X.T. Shen, K.Z. Li, H.J. Li, H.Y. Du, W.F. Cao, F.T. Lan, Microstructure and ablation properties of zirconium carbide doped carbon/carbon composites, Carbon 48 (2010) 344–351.
[4] E.L. Corral, L.S. Wslker, Improved ablation resistance of C–C composites using zirconium diboride and boron carbide, Journal of the European Ceramic Society 30 (2010) 2357–2364.
[5] Y.G. Wang, X.J. Zhu, L.T. Zhang, L.F. Cheng, Reaction kinetics and ablation properties of C/C–ZrC composites fabricated by reactive melt infiltration, Ceramics International 37 (2011) 1277–1283.
[6] Y.G. Tong, S.X. Bai, K. Chen, C/C–ZrC composites prepared by chemical vapor infiltration combined with alloyed reactive melt infiltration, Ceramics International 38 (2012) 5723–5730.
[7] Y.L. Zhu, S. Wang, W. Li, S.M. Zhang, Z.H. Chen, Preparation of carbon fiber-reinforced zirconium carbide matrix composites by reactive melt infiltration at relative low temperature, Scripta Materialia 67 (2012) 822–825.
[8] W. Sun, X. Xiong, B.Y. Huang, G.D. Li, H.B. Zhang, Z.K. Chen, X.L. Zheng, ZrC ablation protective coating for carbon/carbon composites, Carbon 47 (2009) 3365–3380.
[9] H. Wu, H.J. Li, Q.G. Fu, D.J. Yao, Y.J. Wang, C. Ma, et al., Microstructures and ablation resistance of ZrC coating for SiC-coated carbon/carbon composites prepared by supersonic plasma spraying, Journal of Thermal Spray Technology 20 (2011) 1286–1291.
[10] D.D. Jayaseelan, R.G. Sa, P. Brown, W.E. Lee, Reactive infiltration processing (RIP) of ultra high temperature ceramics (UHTC) into porous C/C composites tubes, Journal of the European Ceramic Society 31 (2011) 361–368.
[11] Q.G. Li, S.M. Dong, Z. Wang, G.P. Shi, Fabrication and properties of 3-D C_f/ZrB_2–ZrC–SiC composites via polymer infiltration and pyrolysis, Ceramics International 39 (2013) 5937–5941.
[12] Q.F. Tong, J.L. Shi, Y.Z. Song, Q.G. Guo, L. Liu, Resistance to ablation of pitch-derived ZrC/C composites, Carbon 42 (2004) 2495–2500.
[13] X.T. Shen, K.Z. Li, H.J. Li, Q.G. Fu, S.P. Li, F. Deng, The effect of zirconium carbide on ablation of carbon/carbon composites under an oxyacetylene flame, Corrosion Science 53 (2011) 105–112.
[14] H.H. Sun, H.J. Li, X.T. Shen, G.X. Cao, X.F. Qiang, X.B. Ren, et al., Microstructure and ablation behavior of C/C composites doped with ZrB_2, Journal of Inorganic Materials 26 (2011) 669–672.
[15] D. Zhao, C.R. Zhang, H.F. Hu, Y.D. Zhang, Ablation behavior and mechanism of 3D C/ZrC composite in oxyacetylene torch environment, Composites Science and Technology 71 (2011) 1392–1396.
[16] H.L. Pi, S.W. Fan, Y.G. Wang, C/SiC–ZrB_2–ZrC composites fabricated by reactive melt infiltration with $ZrSi_2$ alloy, Ceramics International, 38, 6458–6541.
[17] K.Z. Li, J. Xie, Q.G. Fu, H.J. Li, L.J. Guo, Effects of porous C/C density on the densification behavior and ablation property of C/C–ZrC–SiC composites, Carbon 57 (2013) 161–168.
[18] X. Zou, Q.G. Fu, L. Liu, H.J. Li, Y.J. Wang, X.Y. Yao, Z.B. He, ZrB_2-SiC coating to protect carbon/carbon composites against ablation, Surface and Coatings Technology 226 (2013), 17–21.
[19] S.A. Chen, C.R. Zhang, Y.D. Zhang, D. Zhao, H.F. Hu, Z.B. Zhang, Mechanism of ablation of 3D C/ZrC–SiC composites under an oxyacetylene flame, Corrosion Science 68 (2013) 168–175.
[20] Y.G. Wang, X.J. Zhu, L.T. Zhang, L.F. Cheng, C/C–SiC–ZrC composites fabricated by reactive melt infiltration with $Si_{0.87}Zr_{0.13}$ alloy, Ceramics International 38 (2012) 4337–4343.
[21] Z.Q. Li, H.J. Li, S.Y. Zhang, J. Wang, W. Li, F.J. Sun, Effect of reaction melt infiltration temperature on the ablation properties of 2D C/C–SiC–ZrC composites, Corrosion Science 58 (2012) 12–19.
[22] W. Li, Y. Xiang, S. Wang, Y. Ma, Z.H. Chen, Ablation behavior of three-dimensional braided C/SiC composites by oxyacetylene torch under different environment, Ceramics International 39 (2013) 463–468.
[23] G.M. Song, S.B. Li, C.X. Zhao, W.G. Sloof, S. Zwaag, Y.T. Pei, J.T.M. D. Hosson, Ultra-high temperature ablation behavior of Ti_2AlC ceramics under an oxyacetylene flame, Journal of the European Ceramic Society 31 (2011) 855–862.
[24] S. Singh, V.K. Srivastava, Effect of oxidation on elastic modulus of C/C–SiC composites, Materials Science and Engineering: A 486 (2008) 534–539.
[25] L. Liu, H. J. Li, W. Feng, X. H. Shi, K. Z. Li, L. J. Guo, Ablation in different heat fluxes of C/C composites modified by ZrB_2-ZrC and ZrB_2-ZrC-SiC particles, Corrosion Science 74 (2013), 159–167.
[26] Z.F. Chen, D. Fang, Y.L. Miao, B. Yan, Comparison of morphology and microstructure of ablation centre of C/SiC composites by oxyacetylene torch at 2900 and 3550 °C, Corrosion Science 50 (2008) 3378–3381.
[27] D. Fang, Z.F. Chen, Y.D. Song, Z.G. Sun, Morphology and microstructure of 2.5 dimension C/SiC composites ablated by oxyacetylene torch, Ceramics International 35 (2009) 1249–1253.
[28] J.C. Han, P. Hu, X.H. Zhang, S.H. Meng, W.B. Han, Oxidation-resistant ZrB_2–SiC composites at 2200 °C, Composites Science and Technology 68 (2008) 799–806.
[29] P. Hu, G.L. Wang, W. Zhi, Oxidation mechanism and resistance of ZrB_2–SiC composites, Corrosion Science 51 (2009) 2724–2732.
[30] J. Xie, K.Z. Li, H.J. Li, Q.G. Fu, L.J. Guo, Ablation behavior and mechanism of C.C–ZrC–SiC composites under an oxyacetylene torch at 3000 °C, Ceramics International 39 (2013) 4171–4178.